Passive acoustic monitoring of a natural CO_2 seep site - implications for Carbon Capture and Storage

Jianghui Li[a,*], Ben Roche[b], Jonathan M. Bull[b], Paul R. White[a], John W. Davis[b], Michele Deponte[c], Emiliano Gordini[c], Diego Cotterle[c]

[a] *Institute of Sound and Vibration Research, University of Southampton, Southampton SO17 1BJ, U.K.*
[b] *Ocean and Earth Science, University of Southampton, National Oceanography Centre, Southampton SO14 3ZH, U.K.*
[c] *National Institute of Oceanography and Applied Geophysics, 34010 Sgonico TS, Italy*

Abstract

Estimating the range at which an acoustic receiver can detect greenhouse gas (e.g., CO_2) leakage from the sub-seabed is essential for determining whether passive acoustic techniques can be an effective environmental monitoring tool above marine carbon storage sites. Here we report results from a shallow water experiment completed offshore the island of Panarea, Sicily, at a natural CO_2 vent site, where the ability of passive acoustics to detect and quantify gas flux was determined at different distances. Cross-correlation methods determined the time of arrival for different travel paths which were confirmed by acoustic modelling. We develop an approach to quantify vent bubble size and gas flux. Inversion of the acoustic data was completed using the modelled impulse response to provide equivalent propagation ranges rather than physical ranges. The results show that our approach is capable of detecting a CO_2 bubble plume with a gas flux rate of 2.3 L/min at ranges of up to 8 m, and determining gas flux and bubble size accurately at ranges of up to 4 m in shallow water, where the bubble sound pressure is 10 dB above that of the ambient noise.

Keywords: `Bubble transect, underwater acoustics, multipath, greenhouse gas, Marine Carbon Capture and Storage`

1. Introduction

In recent years, the storage of carbon dioxide (CO_2) within sub-seabed reservoir has been discussed and identified as an important strategy to mitigate the increase in global temperature due to the increase in atmospheric CO_2 [1, 2, 3, 4]. Many studies have acknowledged that effective monitoring techniques for potential CO_2 gas seepage through the seabed, above Carbon Capture and Storage (CCS) complexes, are essential [5, 6, 7, 8, 9, 10, 11, 12, 13, 14, 15, 16, 17]. Gas bubbles within the seabed migrate, as a result of buoyancy, through a variety of possible pathways to the surface of the seafloor, where they escape into the overlying ocean [18]. As the bubbles become entrained in the water they undergo volume oscillations which radiate sound into the environment [19] which can be used to detect and quantify the gas flux [6]. This paper explores the effectiveness of passive acoustic monitoring for sites above marine CCS storage reservoirs by completing an experiment over a natural CO_2 seep offshore Panarea.

Marine monitoring strategies of CO_2 gas seeps using acoustics include time-lapse acoustic investigations using single/multi-beam echosounders [7, 20] and horizontal backscattering solutions [21]. Active methods are well suited to detection of gas seepage, particularly for gases with low solubility, e.g., methane (CH_4). While for gases possessing higher solubility, such as the CO_2, the dimensions (height and width) of any emerging gas plume would be smaller, making the detection of leakage/seepage with an active acoustic approach more difficult. Further, accurate quantification using active methods requires the use of sonar(s) with a broad range of frequencies, typically in the kHz range for exciting mm-scale bubbles [22]. An alternative approach is to adopt passive acoustic methods to investigate the gas seepage from subsea installations [7, 10, 23]. The most common passive acoustic approach is to measure acoustic sound radiated from gas seeps at a reference point which is close to the leak location [6, 10, 24]. However there has been relatively little work to determine

*Corresponding author: Jianghui Li

the distances at which passive acoustics can detect bubbles emerging from the seabed, or determine at what offsets the inversion of the recorded signal yields accurate estimates of gas flux. There are usually two ways of looking at the passive assessment of flux: (1) in the case of low flux rate, i.e., individual bubbles can be clearly identified based on their resonant frequency, we can use their frequency without the strength of emission; (2) in the case of high flux rate, i.e., individual bubbles cannot be clearly identified, then the sound spectrum is used. Here we investigate the higher flux rate case.

For gas flux determination, the sound pressure level of CO_2 bubbles emitted from the seeps can be measured directly using a hydrophone. Based on the measured pressure level and analysis of sound frequency spectrum, the size distribution and population of CO_2 bubbles emitted from the seafloor seeps can be estimated using passive acoustic inversion [6, 10, 24]. Leighton and White [6] used a spherical spreading law to determine the monitoring range and gas flux, which simplifies the channel acoustic propagation and is incapable of incorporating surface- and bottom-reflected arrivals, which may be particularly significant in shallow water. The effectiveness of passive acoustics for *in situ* monitoring may be reduced due to the dynamic ambient environment, anthropogenic noise, noise from marine organisms, and its deployment may be restricted due to channel obstacles, ocean dynamics [25], acoustic attenuation, bathymetry, and multipath propagation [26, 27, 28, 29]. Thus the low intensity sounds emitted by the bubbles relative to background ocean noise means that passive acoustic monitoring is usually conducted at distances close to gas seeps.

In this study, a field experiment was conducted using an acoustic recorder with multiple hydrophones deployed at various distances from a natural CO_2 gas seep, to investigate the effectiveness of passive acoustics for detecting and quantifying bubble sound arrivals as a function of range. An additional goal was to understand potential interference factors on bubble monitoring. In free space, the sound propagation can be considered as spherical spreading without reflection from channel boundaries. While in an underwater acoustic channel, the sea surface and seabed may act as reflection boundaries; we call the length of the actual propagation path as the channel equivalent range. To find the equivalent range for gas flux determination in shallow water, considering channel multipath and attenuation, we develop a model based on ray-tracing to match acoustic arrivals at each hydrophone location.

The CO_2 vent sites offshore Panarea, Italy are similar to possible leakage scenarios from sub-seabed reservoirs in shelf areas [30] albeit in waters which are shallower than those typical of sites proposed for marine CCS schemes. It provides an ideal natural laboratory [31], for the investigation of CCS leakage detection and monitoring strategies. Here we describe the deployment of the acoustic recorder offshore Panarea and techniques as well as modelling used to process the acoustic data (Section 2). Then we report the results (Section 3) obtained from the deployment along a transect near a selected natural CO_2 gas seep. These field results, i.e., acoustic channel multipath structure, gas plume detection, gas flux and bubble size determination, are used to illustrate the potential of our passive acoustic approach for CCS gas leakage detection and quantification in real shallow water scenarios. We discuss the applicability of using the developed techniques in deeper water as one of the strategies for leakage monitoring of marine carbon storages sites in Section 4.

2. Materials and Methods

2.1. Study site

Panarea, located in the southern Tyrrhenian Sea, is an island within the 200 km long Aeolian Arc, parallel to the continental slope of north coast of Sicily and western coast of Calabria [23, 30, 32, 33, 34, 35, 36]. Figure 1 shows the Panarea and the small islets situated to the east. The island and these islets are the emergent parts rising from the western section of a submarine stratovolcano [30, 37, 38]. The stratovolcano is over 1200 m in height [39] and 20 km in width [40]. Many volcanic craters are visible on the seabed, and a complex fracture system has been imaged with an overall SW-NE orientation which may link Panarea with a nearby volcano island Stromboli in the northeast direction.

The islets east of Panarea are situated on a shallow plateau with water depth of 30 m [33, 41], where extensive fluid exhalations into the water column occur from the volcanic activity. Numerous gas leakages have been measured, with relatively stable composition of around 98% CO_2, 1.7% H_2S and other trace gases

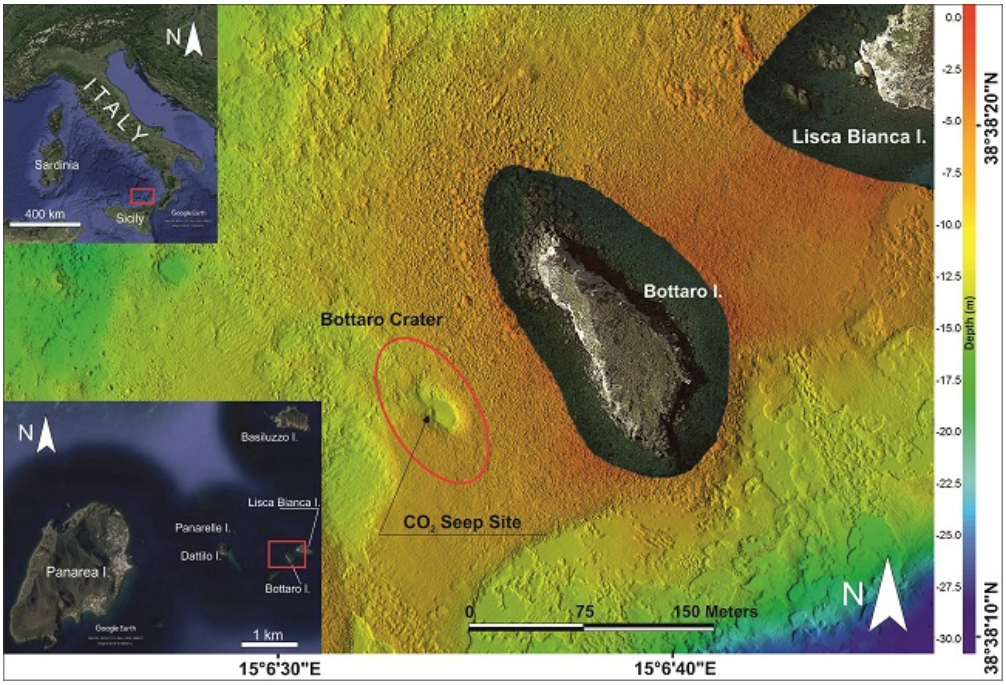

Figure 1: Maps showing the position of the CO_2 seep site offshore Panarea (c. 100 m west of Bottaro Islet in 12.5 m water depth). The position of the ∼10 cm wide pockmark is indicated in the red circle.

(N_2, He, H_2, CH_4) [34, 42, 43, 44], while flux rates vary from different gas seeps. These natural gas release seeps and the CO_2-rich gas composition make the area offshore Panarea an excellent test bed to study gas leakage scenarios and detection methods. Previous studies offshore Panarea have mapped [45, 46] the rising (CO_2 and CH_4) gas plumes at 80 different locations [30]; and continuous acoustic monitoring of bubble flux has been conducted [47]. However, there has been no investigation of the distances from a seep site at which gaseous CO_2 can be detected and/or quantified using passive acoustics.

In this study, a volcanic crater (Bottaro Crater) generates a number of continuous CO_2-rich gas bubbles streams (Figure 2(b)). We chose to investigate a seep in 12.5 m water depth close to the rim of the crater, with a minimum distance of 20 m to other comparable bubble streams, and designed an experimental geometry that ran perpendicular to the crater edge. As well as making acoustic measurements at different distances, we used a diver-controlled funnel to directly measure the gas flux. To measure the real size of the rising bubbles, we used high-quality underwater video equipment (SONY FDR-X3000 Action Camera, with UltraHD resolution 4K (3840×2160) at 30p).

2.2. Acoustic receiver deployment

Two hydrophones linked to an acoustic recorder (*RS ORCA*) measured the sound of bubbles emerging from the seabed at different ranges. These hydrophones were absolutely calibrated with receive sensitivity of -164.5 dB re: 1 V/μPa. A gain of 15 dB data was applied to each recording channel, and a sampling frequency of 96 kHz was used. Data presented here was collected on May 16th 2018 when winds were light, sea state <2 on the Beaufort scale.

Figure 2(a) shows the cartoon experimental geometry on the edge of Bottaro Crater. To minimize the acoustic propagation effect caused by seabed grasses or rocks (Figure 2(b)), each hydrophone was fixed on a securely positioned tripod on the seafloor at a height of 0.75 m. In the experiment, one hydrophone closest to the seep location at 0.3 m was used as the reference hydrophone and remained at a fixed location, whilst the other hydrophone was moved to various ranges to form a transect. The different acoustic channels were

synchronously recorded. Acoustic measurements were conducted at horizontal distances between 0.3 m and 8 m away from the centre of the seep site.

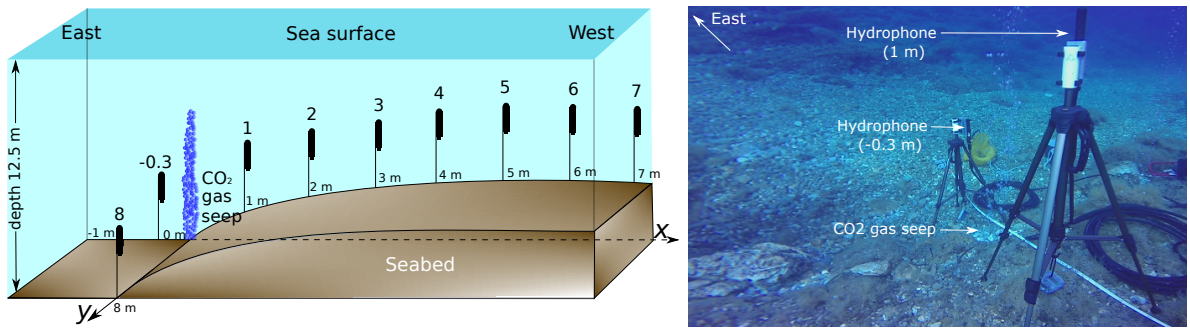

(a) (b)

Figure 2: Experimental geometry over natural CO_2 seep on the western edge of Battaro Crater. (a) Overall experiment geometry showing the locations of the seep and hydrophone measurement positions. The transect was orientated east to west perpendicular to the edge of the crater. The seabed rose gently out of the crater to the west. An additional measurement was made at right angles to the transect at an offset of 8 m. (b) Underwater image of the central part of the experiment transects showing the reference hydrophone at 0.3 m and a transect hydrophone at 1 m from the seep.

2.3. Signal processing and modelling

The approach to the bubble detection and quantification is shown in the block diagram Figure 3. Measured data from the reference hydrophone (0.3 m away from the centre of the seep) is cross-correlated with measured data from the other transect locations to determine the travel times and ray paths for the sound emitted by bubbles emerging from the seabed for gas plume detection. Prior to the quantification of the gas flux, ray trace modelling using the Bellhop Acoustics Toolbox [48] is completed to obtain the channel impulse response for each hydrophone location along the transect. The impulse response is compared and corrected for the multipath structure derived from the bubble detection. The equivalent range for each hydrophone location from the centre of the seep corresponding to the channel impulse response, is applied into the passive inversion model [6] to compute the gas flux and bubble size distribution and bubble numbers, and then gas flux. After we obtain the bubble size distribution and bubble numbers, we transfer it into a bubble forward model to generate modelled hydrophone data for comparison with the measured hydrophone data.

2.3.1. Ray trace based modelling

Ray trace modeling was used to compute the transmission loss and channel impulse responses [48]. The sea surface was calm during the experiment, thus we assume the sea surface as flat in the simulation. The simulation incorporates the bathymetry shown in Figure 2(a), the sound speed profile (SSP) shown in Figure 4(a), and a central frequency of 350 Hz. The depth of the bubble sound source is at 12.5 m, and the positions of the transect hydrophone are set according to the deployment locations shown in Figure 2(a). The bubble is much smaller than the wavelength of the sound radiated so is well-characterized as an omni-directional acoustic source. The seabed composition is a mixture of sands and gravels (Figure 2(b)), and we used an estimate of ∼0.7 dB per wavelength attenuation [49].

We first carry out multiple runs to determine the channel impulse responses and the time delay of each arrival at the hydrophone positions. The arrival structure from the model (i.e., channel impulse responses), corresponding to the multipath arrivals, are then compared with the delays computed from the cross-correlation between reference field data and transect field data. As the measured sound arrived via multiple paths, these results are used to compute the equivalent propagation range $\hat{r}$:

$$\hat{r} = \frac{r_0 \bar{A}_0}{\sum_{i=1}^{I} A_i}, i = 1, \ldots, I, \tag{1}$$

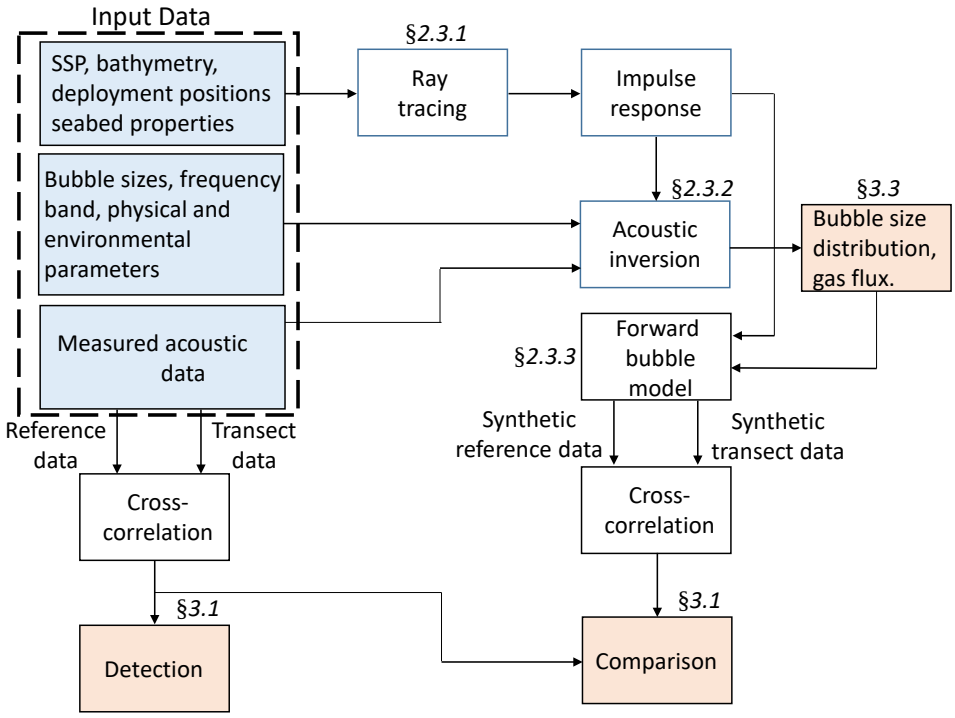

Figure 3: Block diagram of the approach to bubble/gas flux detection, quantification, and verification. Inputs are shown in blue colour, and outputs are shown in red colour. The steps are numbered corresponding to the paragraphs in the main text. For more details on the bubble passive inversion model see [6, 10, 24].

where r_0 is the range of a reference point with sound signal arriving only from the direct path, $\bar{A}_0$ is the path impulse amplitude received at the reference point, I is the number of multipath, and A_i is the amplitude of the path impulse response for each arrival, usually overlapped temporally in shallow water, considering reflection from sea surface and ocean bottom with phase shift.

2.3.2. Passive inversion model

For inversion of the gas flux from the bubble stream, we identify the frequency range, $[f_{\min}, f_{\max}]$ over which the sound of the bubbles is evident above the ambient noise field. Ambient condition were measured well away from any seep site location. The radii of the bubbles whose resonant frequencies correspond to $f_{\min}$ and $f_{\max}$ are identified as $R_{\max}$ and $R_{\min}$ respectively [50], according to the low-amplitude pulsations occur at a natural angular frequency $\omega_0 (= 2\pi f)$, which is given by [50]:

$$\omega_0 = \frac{1}{R_0\sqrt{\rho_0}}\sqrt{3\kappa\left(p_0 - p_v + \frac{2\sigma}{R_0}\right) - \frac{2\sigma}{R_0} + p_v - \frac{4\eta^2}{\rho_0 R_0^2}}, \tag{2}$$

where $R_0 \in [R_{\min}\ R_{\max}]$ is the bubble equilibrium radius [m], ρ_0 is the ambient liquid density [kg/m^3], p_0 is the ambient pressure [Pa], p_v is the vapor pressure [Pa], σ is the surface tension [N/m], η is the shear viscosity [Pa.s], and κ is the ratio of specific heat of the gas at constant pressure to that at constant volume, depending on whether the gas is behaving adiabatically, isothermally, or in some intermediate manner [51].

Then we create a bin vector of the radii R_0 with a bin width of $(R_{\max}\text{-}R_{\min})/M$, where M is the number of bins. For each bin, we integrate the measured power spectral density (PSD) across the frequency range

corresponding to the resonant frequencies of the radii in the bin [6]. The modelled spectrum of a single bubble emission is given by [6]:

$$|X_b(\omega; R_0)|^2 = 2\left[(\omega_0^2 R_0^3)\frac{\rho_0}{\hat{r}}\frac{R_{\varepsilon 0i}}{R_0}\right]^2 \times \left(\frac{4[(\omega_0\delta_{tot})^2 + 4\omega^2]}{[(\omega_0\delta_{tot})^2 + 4(\omega-\omega_0)^2][(\omega_0\delta_{tot})^2 + 4(\omega+\omega_0)^2]}\right), \tag{3}$$

where $R_{\varepsilon 0i}/R_0$ is the initial amplitude of displacement of the bubble wall at the start of the emission as a proportion of the equilibrium bubble radius (see more details in [6]). Here, we assume this ratio is constant to facilitate the inversion [5]. δ_{tot} is the total dimensionless damping coefficient at bubble natural frequency [50], and $\hat{r}$ is the equivalent range computed from Eq.(1).

If the acoustic emissions of the bubbles are all uncorrelated, then the PSD $S(\omega)$, of the far-field acoustic signature of the bubble cloud can be expressed as

$$S(\omega) = \int_{R_0=R_{\min}}^{R_{\max}} D(R_0)|X_b(\omega; R_0)|^2 dR_0, \tag{4}$$

where $D(R_0)$ is the bubble-emission size distribution as a function of the bubble radii R_0. Based on the computed acoustic pressure, we estimate the bubble size distribution and population from the recorded passive acoustic data, and solve Eq.(4) using the passive acoustic inverse method proposed by Leighton and White [6]. Thus, the probability density function (PDF) of bubble equilibrium radius $p_{\mathrm{b}}^{R_0}$ as well as number of bubbles for each size are obtained, and the gas flow rate F [L/min] is then computed as

$$F = \sum_{R_0=R_{\min}}^{R_{\max}} \frac{4}{3}\pi R_0^3 D(R_0). \tag{5}$$

Note that the pressure in the model [6] is computed using spherical spreading, which is not applicable in shallow water channels where multipath effects should not be neglected. To make the inversion method applicable in shallow water, we use the equivalent range $\hat{r}$ (Eq.(1)).

2.3.3. Forward modelling of bubble plume sound field

The inverted PDF of bubble equilibrium radius $p_{\mathrm{b}}^{R_0}$ and bubble numbers are used to generate a forward model. For a single bubble emitted from a seep, we assume the bubble oscillates in a limit of small amplitude $|R_\varepsilon| \ll R_0$, which is valid for most ocean gas bubbles pulsating at their natural frequencies [52]. The oscillatory acoustic pressure signature in the liquid $P_{\mathrm{b}1}(t)$ of the monopole emission detected at time t by a hydrophone in the far field for a single pulsating bubble, is given by [6]:

$$P_{\mathrm{b}1}^{R_0}(t, t_i) = (\omega_0 R_0)^2 \frac{\rho_0}{r_1} R_{\varepsilon 0i} e^{-\omega_0 \delta_{tot}(t-t_i)/2} \times H(t-t_i)\cos\omega_0(t-t_i), \tag{6}$$

where t_i is the time at which the acoustic signal is first detected at the monitor, H is the Heaviside step function, and r_1 is the reference range (1 m adopted here) from the bubble acoustic centre. Low-amplitude pulsations occur at a natural angular frequency ω_0, which is given by Eq.(2) [50].

If the acoustic emissions of the bubbles are all uncorrelated, then the far-field acoustic signature of the bubble cloud (gas flux) can be expressed as [24]

$$P_{\mathrm{b}1}(t) = \sum_{i=1}^{N_{\mathrm{b}}} P_{b1}^{R_0}(t, t_i), t_i \in [0\ T_{\mathrm{b}}], \tag{7}$$

where t_i is randomly distributed in the interval $[0\ T_{\mathrm{b}}]$, following the bubble radius PDF $p_{\mathrm{b}}^{R_0}$. Since we have now constructed time series of bubble singles, we convolve them with channel impulse responses and compute the reference/transect cross-correlation.

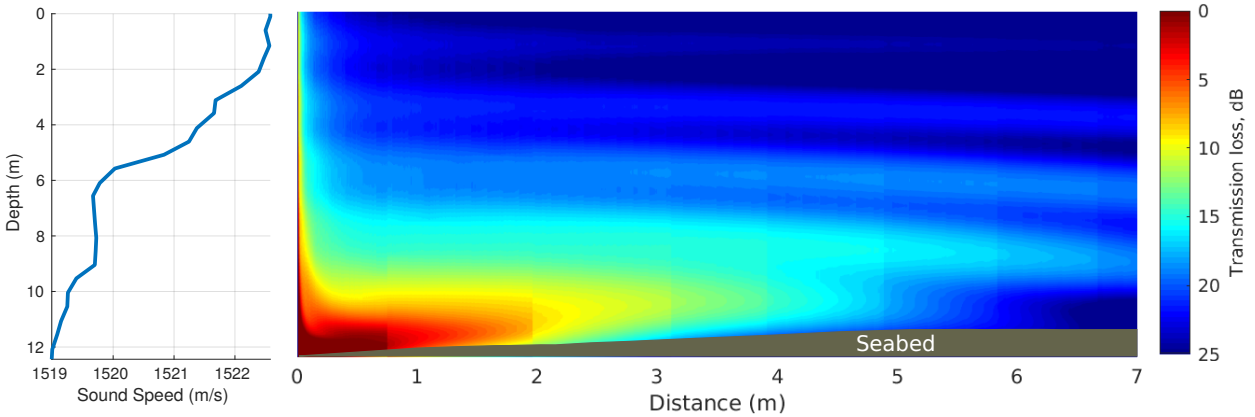

(a) (b)

Figure 4: Sound speed profile (SSP) collected on May 16th 2018 in the Panarea water area, and transmission loss within 7 m in the acoustic channel calculated using Bellhop. The seep site radiating bubble sound is at a depth of 12.5 m. (a) Sound speed profile; (b) Transmission loss structure at 350 Hz.

3. Results and discussion

At the seep site on the edge of Bottaro Crater, gas bubbles leaked from a seabed consisting of sands, gravels, and patches of sea grass (Figure 2(b)). The CO_2 emerged from a small circular pockmark of radius about 10 cm. The approach used to estimate the CO_2 flux from the seep considers the acoustic data recorded at different distances together with direct measurement of the flux. We determined how bubble sound propagates in the water column, then matched our modelling results to the field data, before determining the flux using the inversion approach. The SSP measured at the field site is shown in Figure 4(a), and the modelled transmission loss (TL) structure using the SSP at 350 Hz (frequency peak of the measured bubble sound) is shown in Figure 4(b), showing complex channel propagation and the TL structure.

3.1. Bubble sound field observations and arrival paths

For each distance of a hydrophone from the seep site, cross-correlation of the reference acoustic field data at -0.3 m (sound predominantly from the gas seep) with the measured sound field was used to identify the major arrival paths (Figure 5(a)) by matching with the impulse response derived from Bellhop ray-tracing modelling (Figure 5(b), discussed in Section 3.3). The seep site bubble field is detected by the hydrophones from both the direct arrival and the water surface reflection at distances of 2 to 8 m. The direct path is well modelled (Figure 5(b)) at all offset distances, while the water-surface reflection is best-modelled where the path amplitudes are the strongest (6 and 7 m).

The strength of the direct path signal decreases as the transect distance increases, and the normalized amplitudes show that the acoustic attenuation through direct propagation path is significant. Moreover, the direct path signal is greater than the reflected signal at distances up to 4 m, while the power strength of surface reflected path signal is greater than that of the direct ones at 6-7 m. At distances of 5 m and perpendicular 8 m the signals from the two paths are comparable where the Lloyd's mirror effect (discussed in Section 3.2) [53] is the strongest. As the transect distance increases, the delay for the direct path increases linearly, while the delay of reflected path does not.

To validate the multipath propagation along the transect, we estimated coordinates for each transect hydrophone from the delays for each path (direct/reflected) and compute the difference between physical length of the propagation path from the delays. Table 1 shows the results comparing the average delays calculated from cross-correlations and from measured positions of the hydrophones relative to the seep. It is seen that the error for each path calculation is less than 7%.

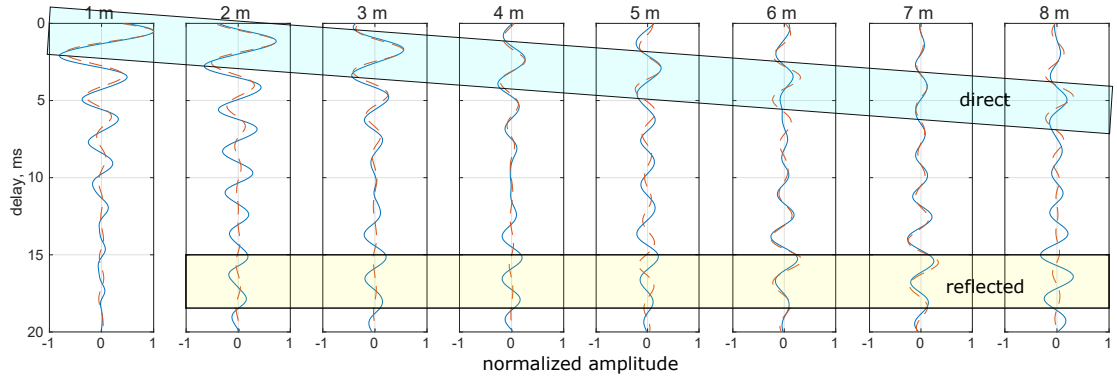

(a)

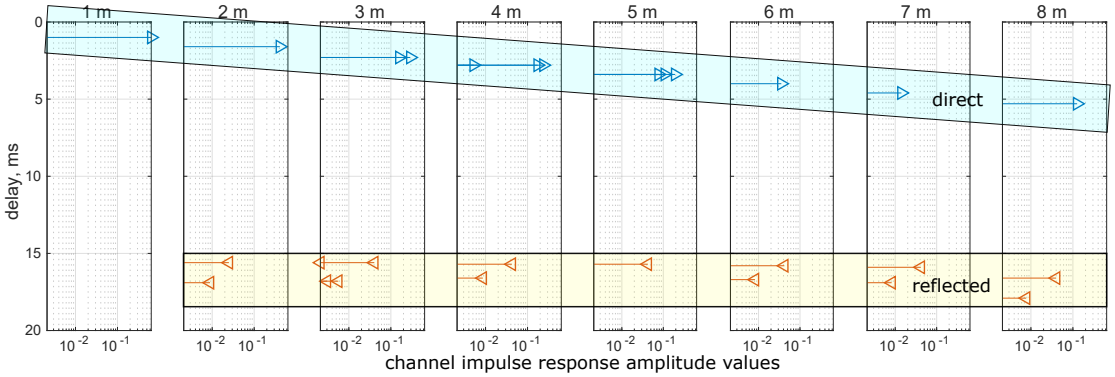

(b)

Figure 5: Observations and modelled impulse response at different distances from the CO2 seep site. (a) Observed sound field at different offsets (blue) and matched synthetic trace (red). The amplitude at each distance is normalised to the peak value in the cross-correlation at an offset of 1 m. (b) Impulse response derived from ray-tracing used to produce the synthetic. The direct arrivals are indicated within the blue box, while the arrival that results from a reflection at the water-surface is within the yellow box.

3.2. Spectral analysis

Continuous monitoring at a constant range from the seep site to the hydrophone yielded a concentrated interval of acoustic signal in the frequency domain, providing an initial frequency interval $[f_{\min}\ f_{\max}]$ for gas flux and bubble size determination. Figure 6(a) shows the spectrogram from measured hydrophone data at -0.3 m for 32 minutes. It is seen that the majority of the acoustic energy from the bubbles lies on a fairly broad frequency band 150-800 Hz, peaking at about 350 Hz.

Table 1: Bubble sound propagation and range estimation from average delays estimated by cross-correlation between the transect data (1-8 m) and the reflected data measured at -0.3 m. Propagation multipath include direct path and sea surface reflected path.

Transect	path	delay	length	error
1 m with -0.3 m	direct	0.47 ms	0.70 m	2.9%
2 m with -0.3 m	direct	1.06 ms	1.60 m	3.2%
	reflect	16.29 ms	24.44 m	
3 m with -0.3 m	direct	1.74 ms	2.63 m	6.4%
	reflect	16.54 ms	24.81 m	
4 m with -0.3 m	direct	2.24 ms	3.38 m	5.9%
	reflect	16.56 ms	24.84 m	
5 m with -0.3 m	direct	2.83 ms	4.28 m	3.8%
	reflect	16.63 ms	24.94 m	
6 m with -0.3 m	direct	3.49 ms	5.27 m	6.7%
	reflect	16.69 ms	25.03 m	
7 m with -0.3 m	direct	4.02 ms	6.07 m	3.8%
	reflect	16.78 ms	25.17 m	
8 m with -0.3 m	direct	4.82 ms	7.28 m	4.3%
	reflect	17.84 ms	26.76 m	

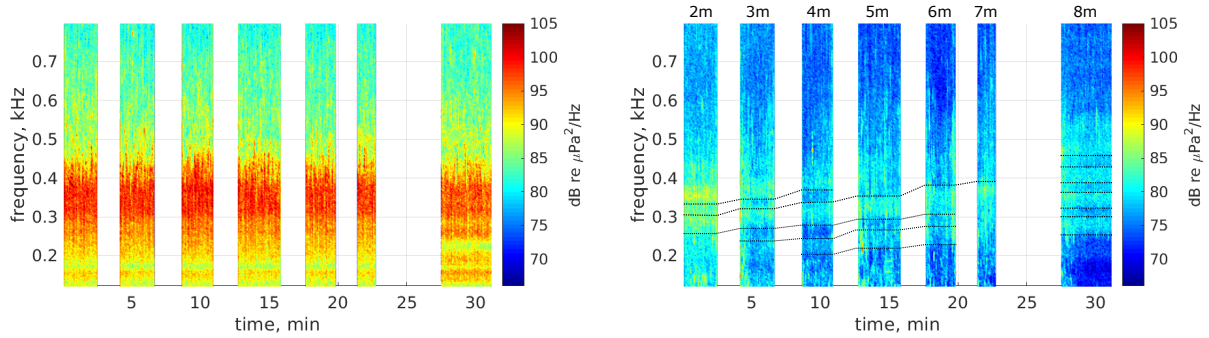

(a) reference -0.3 m.

(b) transect 2-7 m, and 8 m perpendicular

Figure 6: Spectrograms from measured hydrophone data. (a) shows the frequency interval of interest 150-800 Hz; (b) shows the outline of Lloyd's mirror effect which can be observed from the spectrum marked as dashed lines. Recorded sound with noise introduced by divers conducting the hydrophone transect has been removed and is shown as blank in the figures.

Figure 7 shows power spectral density (PSD) of the measured sound at ranges from -0.3 m to 4 m, and the ambient noise in this area without gas seeps observed. As the transect distance increases, the PSD of the measured sound decreases accordingly. Li et al. [24] concluded that for accurate field gas bubble sound detection and determination, the signal to noise ratio (SNR) should be at least 6 dB. In the shallow water case, where the effect from the sea surface and ambient are significant, the SNR should be higher than 6 dB, i.e., the PSD at 4 m is average ∼10 dB higher than that of the ambient noise in the frequency of interest (Figure 7).

It should be noted that, as the transect distance increased from the seep site, constructive and destructive

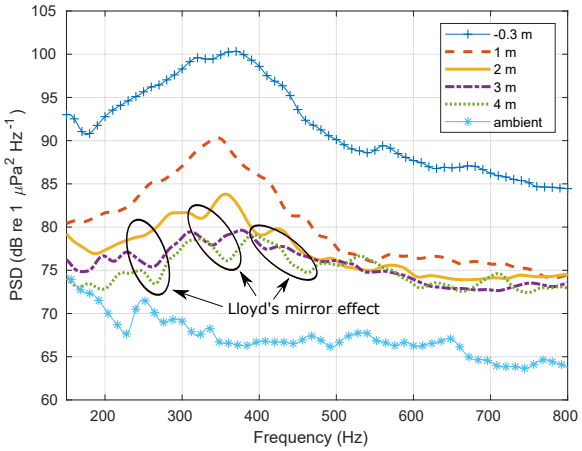

Figure 7: Power spectral density (PSD) of the sound recorded at different distances from the CO_2 seep site. Frequencies between 150 and 800 Hz record bubble sounds, with sound level decreasing with distance from the seep. The solid circles indicate distances and frequencies affected by the Lloyd's mirror effect. The PSD at transect 4 m is measured as ∼10 dB higher than that of the ambient noise.

interference between the direct path and reflected path forms the Lloyd's mirror effect [53], plotted as dashed lines in Figure 6(b) and dashed circles in Figure 7. Such effect can cause significant interference on passive acoustic monitoring in shallow water, especially on the bubble size determination at low frequencies (<500 Hz), because sea surface sound reflections are nearly 180 degrees out of phase with the direct sound arrivals. Bubble sounds at some part of low-frequency spectrum were not measured, shown as weak PSD in the dashed circles, which is due to the interference from Lloyd's mirror effect. This has been incorporated in the analysis by considering the multipath propagation using the channel impulse response derived equivalent range to replace the physical range for each transect.

3.3. Gas flux and bubble size

The gas flux and CO_2 bubble size distribution were quantified by passive acoustic inversion. The time taken for the CO_2 to fill a 2-litre plastic measuring cylinder was used to directly determine the gas flux from our studied seep site. Repeated measurements by divers allowed an average fill time of 53 seconds to be determined, which equates to a flux rate of 2.3 L/min (Figure 8(a)).

3.3.1. Gas flux determination

Figure 9 shows the two examples (4 m and 7 m) of output of the Bellhop ray-tracing model for the east to west bubble transect. Both the direct (blue) and reflected (red) path for the two cases are visible, while the path with both the reflection from the sea surface and seabed are shown in black colour lines. Figure 5(b) shows the modelled channel impulse response as a function of deployment distance. The impulse responses with delay less than 10 ms correspond to the direct path, while those above 10 ms correspond to the propagation path reflected from the sea surface. The impulse response delays match well with the cross-correlation results from the measured acoustic data shown in Figure 5(a) blue line peaks boxed and in Table 1.

We further use the bubble forward model to generate modelled bubble sound and calculate the modelled cross-correlation results for comparison with the measured one. The comparison results are shown in Figure 5(a) red lines. It is seen that the two lines match quite well, particularly at 1-4 m and 6-7 m where the direct path or reflected dominates the propagation. While at 5 m and perpendicular 8 m where the signals' strength from the two path are comparable resulting significant interference from the Lloyd's mirror effect. Unmatched part of the correlation curve can be partly interpreted to the multiple interference bubble

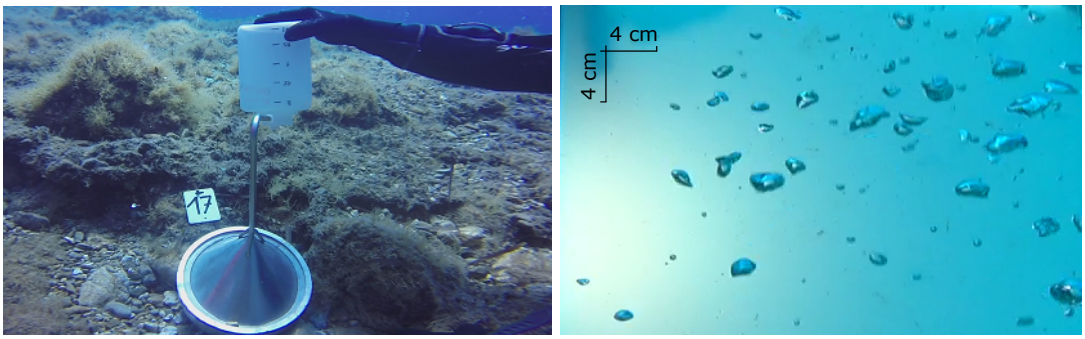

(a) (b)

Figure 8: Experimental scenarios. (a) Gas Bubbles collected for 2-liter in 53 s. Average gas flow rate is 2.3 L/min. (b) Bubble size measurement using underwater camera. The background whiteboard was 18×30 cm in dimension. The distance between the camera and the whiteboard was 1.4 m. The bubble stream was rising ±20 cm mid-way between the camera and the whiteboard.

streams around the measured focused seep site in the experiment while a single bubble seep is considered in the model.

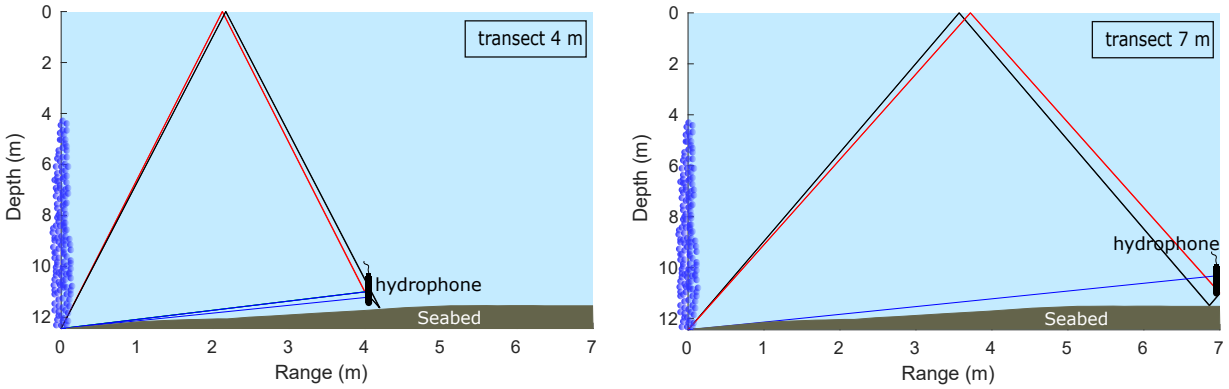

(a) (b)

Figure 9: Examples of Bellhop ray-trace output for the bubble transect over the west side of Bottaro Crater. (a) Transect range 4 m; (b) Transect range 7 m. Both cases show the direct path, the path with only sea surface reflection, and the path with both sea surface and seabed reflection. Black ray hits both boundaries; red ray hits surface only; and blue ray hits bottom only.

As we have the impulse responses for the transect obtained from the ray tracing, we can model the signal at the hydrophones by convolving the signals measured at the reference position with the impulse responses [54]. The frequency spectrum is quite weak from the modelling at distances 5-8 m bubble transect due to the significant attenuation as shown in Figure 4(b), which does not match the observations as shown in Figure 6(b). This is because the level of focused seepage sound at such greater transect distances was less than 10 dB above the ambient environment noise level, and the level of interference sound from other bubble streams was increased. Thus here we are unable to determine the focus bubble gas flux at distance 5-8 m, where the measured acoustic sound was severely influenced by the noise interference.

The comparisons between the gas flux determination from passive acoustic inversion using spherical

spreading range and multipath equivalent range are shown in Table 2. It is seen that the error of gas flux estimation from inversion with spherical spreading is most accurate close to the seep location, with errors up to 41% at other ranges. The accuracy increases significantly when the effects of multipath are included. Taken together, we successfully estimated the gas flux using the inversion method with relatively small errors (<10%) for ranges up to 4 m.

Table 2: Comparison of gas flux estimation results from passive acoustic inversion considering spherical spreading and channel multipath propagation. The diver measured gas flow rate from *in situ* collection is 2.3 L/min.

Field	**spherical**		**multipath**	
range	**flow rate**	**error**	**flow rate**	**error**
-0.3 m	2.2 L/min	4.4%	2.4 L/min	7.1%
1 m	1.8 L/min	18.6%	2.1 L/min	6.2%
2 m	1.3 L/min	40.7%	2.3 L/min	0.0%
3 m	1.5 L/min	32.7%	2.4 L/min	7.1%
4 m	1.7 L/min	23.0%	2.5 L/min	8.8%

3.3.2. Bubble size determination

Figure 10 shows the PDF of the estimated bubble size distribution from passive acoustic inversion at ranges from -0.3 m to 4 m. The radius of CO_2 bubbles emerging from the 12.5 m deep seafloor were mainly between 1 cm and 2.5 cm. Estimated bubble size tends to decrease as the hydrophone ranges increase. The increase in the number of estimated small bubbles with radius less than 1.3 cm is due to the reduced signal to noise ratio in this band, where some of the ambient noise is incorporated with the noise of bubbles being emitted from the seep. The resulting uncertainties are interpreted to be the combination of bubble acoustic attenuation in the channel, the Lloyd's mirror effect and the presence of ambient noise. As the seep/hydrophone distance increases, the frequency band from the Lloyd's mirror effect also shifts, which changes the estimated bubble size.

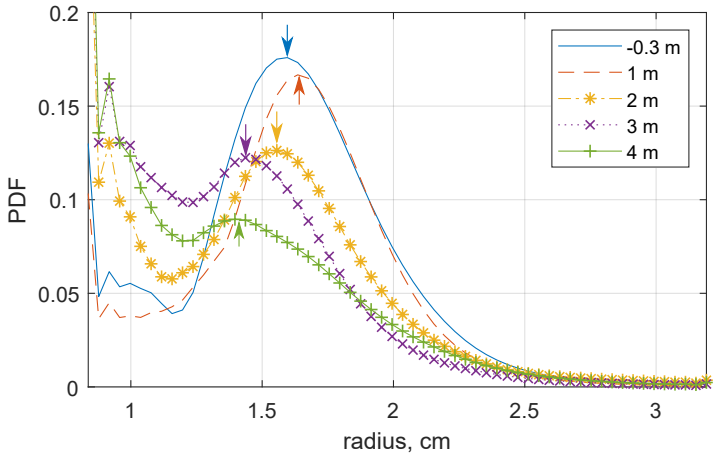

Figure 10: Probability density function (PDF) of the estimated bubble size distribution from passive acoustic inversion at different distances from the CO_2 seep site. Estimated bubble size tends to decrease as the hydrophone ranges increases (peak moves from 1.7 cm (at 1 m) to 1.4 cm (at 4 m) as indicated by arrows). The increase in the number of small bubbles with radius less than 1.3 cm is due to the reduced SNR at greater ranges.

Figure 8(b) shows a horizontal view of the bubble plume, which shows that the radius of majority bubbles were normally between 1 cm and 2.5 cm. This provides agreement between the modelled and measured bubble size and proves the effectiveness of our approach.

4. Conclusions and discussion

The ability of passive acoustic monitoring to detect and quantify continuous natural CO_2 gas leakage from sub-seabed was tested at different ranges in shallow water offshore Panarea island. A CO_2 bubble plume was successfully detected at ranges up to 8 m, and the gas flux and bubble size determined for distances of up to 4 m, where the bubble sound pressure is measured as ∼10 dB higher than that of the ambient noise. The Panarea passive acoustic tests have demonstrated that the passive acoustic inversion method described here, when integrated with scenario modelling is an appropriate and cost-effective approach to be applied in detection and quantification of seabed gas leakage in shallow water.

In particular, the transect data has enabled a definition of multipath propagation (direct or sea surface reflect) of bubble sound in the acoustic channel, and has been used to estimate the gas flux and bubble size distribution. The range at which bubbles can be detected has been limited by multipath propagation, significant attenuation, and interference in underwater acoustic channels. The estimated gas fluxes show agreement within 10% error to the measured gas fluxes, and the estimated bubble sizes are comparable to those observed.

Modelling based on a ray-tracing program considers the multipath propagation, providing relatively accurate equivalent range for gas flux determination up to 4 m in the shallow water scenario investigated. However, there were multiple other bubble seeps around the bubble transect area which increased the sound levels and made the determination of gas flux beyond 4 m for a specific bubble seep unsuccessful. Characterizations of the site-specific source-receiver geometry, bathymetry, bubble plume shape/angle, sediment properties, and sound speed profile are also important before conducting passive acoustic monitoring and are of particular importance when designing monitoring strategies for offshore CCS sites.

The study area at Panarea is in shallower water (12.5 m) than sites normally considered for CCS across the Global Ocean (e.g., [55, 56, 57, 58, 59, 60, 61]), which are in deeper shelf seas. We can still apply the passive acoustic techniques developed here for bubble detection and quantification in deeper water. The applicable

range of such detection and quantification depends of the actual gas flux on the seepage site, the depth of the water, and the ambient noise in the area. The gas flux in this study was 2.3 L/min which results in a detection range up to 8 m and a quantification range up to 4 m. Considering the same ambient noise level and the same emergent gas flux in deeper water, due to the high propagation loss (about 40 dB from the seabed to the sea surface [24]) in the acoustic channel, only the direct acoustic path for the bubble sound would need to be considered, simplifying the analysis. Our methods will be applicable in the deep sea, and for normal ambient noise levels we should be able to detect and quantify sound at greater offset ranges than at Panarea. We are currently analysing data from the STEMM-CCS experiment (`https://www.stemm-ccs.eu/`) in the central North Sea, which included a passive acoustic component, and will be the subject of future publications.

Passive acoustic recorders fixed to the seabed can be linked to battery packs to permit long-period (greater than a year) deployments. The requirement for relatively high sampling rates to record the bubble sounds with sufficient fidelity, means that data volumes are large, and there is no straightforward method to remotely transmit the data without direct cabling; the data is retrieved when the acoustic recorder is recovered. In practical terms the relatively short offset detection ranges for bubble sounds on hydrophones, means that fixed passive acoustic recorders on the seabed will only deployed at sites where there is high risk of gas escape (e.g., seabed installations including abandoned oil and gas wells), or after detection by active acoustic sensors. Additional methods for passive acoustic sensing include deployment on autonomous underwater vehicles, and using distributed acoustic sensing, and both these techniques are the subject of continuing work.

Acknowledgements

Funding was provided by the European Unions Horizon 2020 research and innovation programme under the grant agreement number 654462 (STEMM-CCS). We thank the scientific divers Andrea Fogliozzi and Martina Gaglioti for their professional and tireless work.

References

[1] R. K. Pachauri, M. R. Allen, V. R. Barros, J. Broome, W. Cramer, R. Christ, J. A. Church, L. Clarke, Q. Dahe, P. Dasgupta, et al., Climate change 2014: synthesis report. Contribution of Working Groups I, II and III to the fifth assessment report of the Intergovernmental Panel on Climate Change, IPCC, 2014.

[2] C. Roelofse, T. M. Alves, J. Gafeira, O. O. Kamaldeen, An integrated geological and GIS-based method to assess caprock risk in mature basins proposed for carbon capture and storage, International Journal of Greenhouse Gas Control 80 (2019) 103–122. doi:10.1016/j.ijggc.2018.11.007.

[3] S. Caserini, G. Dolci, A. Azzellino, C. Lanfredi, L. Rigamonti, B. Barreto, M. Grosso, Evaluation of a new technology for carbon dioxide submarine storage in glass capsules, International Journal of Greenhouse Gas Control 60 (2017) 140–155. doi:10.1016/j.ijggc.2017.03.007.

[4] L. Vielstädte, P. Linke, M. Schmidt, S. Sommer, M. Haeckel, M. Braack, K. Wallmann, Footprint and detectability of a well leaking CO2 in the Central North Sea: Implications from a field experiment and numerical modelling, International Journal of Greenhouse Gas Control 84 (2019) 190–203. doi:10.1016/j.ijggc.2019.03.012.

[5] M. Loewen, W. Melville, A model of the sound generated by breaking waves, J. Acoust. Soc. Am. 90 (4) (1991) 2075–2080. doi:10.1121/1.401634.

[6] T. Leighton, P. White, Quantification of undersea gas leaks from carbon capture and storage facilities, from pipelines and from methane seeps, by their acoustic emissions, Proc. R. Soc. A (2011) rspa20110221doi:10.1098/rspa.2011.0221.

[7] J. Blackford, J. M. Bull, M. Cevatoglu, D. Connelly, C. Hauton, R. H. James, A. Lichtschlag, H. Stahl, S. Widdicombe, I. C. Wright, Marine baseline and monitoring strategies for carbon dioxide capture and storage (CCS), International Journal of Greenhouse Gas Control 38 (2015) 221–229. doi:10.1016/j.ijggc.2014.10.004.

[8] L. Mabon, S. Shackley, N. Bower-Bir, Perceptions of sub-seabed carbon dioxide storage in Scotland and implications for policy: a qualitative study, Marine Policy 45 (2014) 9–15. doi:10.1016/j.marpol.2013.11.011.

[9] H. K. Hvidevold, G. Alendal, T. Johannessen, A. Ali, Survey strategies to quantify and optimize detecting probability of a CO_2 seep in a varying marine environment, Environmental Modelling & Software 83 (2016) 303–309. doi:10.1016/j.envsoft.2016.06.006.

[10] B. J. Bergès, T. G. Leighton, P. R. White, Passive acoustic quantification of gas fluxes during controlled gas release experiments, International Journal of Greenhouse Gas Control 38 (2015) 64–79. doi:10.1016/j.ijggc.2015.02.008.

[11] D. Atamanchuk, A. Tengberg, D. Aleynik, P. Fietzek, K. Shitashima, A. Lichtschlag, P. O. Hall, H. Stahl, Detection of CO_2 leakage from a simulated sub-seabed storage site using three different types of pCO_2 sensors, International Journal of Greenhouse Gas Control 38 (2015) 121–134. doi:10.1016/j.ijggc.2014.10.021.

[12] P. Taylor, H. Stahl, M. E. Vardy, J. M. Bull, M. Akhurst, C. Hauton, R. H. James, A. Lichtschlag, D. Long, D. Aleynik, et al., A novel sub-seabed CO_2 release experiment informing monitoring and impact assessment for geological carbon storage, International Journal of Greenhouse Gas Control 38 (2015) 3–17. doi:10.1016/j.ijggc.2014.09.007.

[13] M. Cevatoglu, J. M. Bull, M. E. Vardy, T. M. Gernon, I. C. Wright, D. Long, Gas migration pathways, controlling mechanisms and changes in sediment acoustic properties observed in a controlled sub-seabed CO2 release experiment, International Journal of Greenhouse Gas Control 38 (2015) 26–43. doi:10.1016/j.ijggc.2015.03.005.

[14] K. Shitashima, Y. Maeda, A. Sakamoto, Detection and monitoring of leaked CO2 through sediment, water column and atmosphere in a sub-seabed CCS experiment, International Journal of Greenhouse Gas Control 38 (2015) 135–142. doi:10.1016/j.ijggc.2014.12.011.

[15] C. Kolster, S. Agada, N. Mac Dowell, S. Krevor, The impact of time-varying CO2 injection rate on large scale storage in the UK Bunter Sandstone, International Journal of Greenhouse Gas Control 68 (2018) 77–85. doi:10.1016/j.ijggc.2017.10.011.

[16] A. L. Stork, C. Allmark, A. Curtis, J.-M. Kendall, D. J. White, Assessing the potential to use repeated ambient noise seismic tomography to detect CO2 leaks: Application to the Aquistore storage site, International Journal of Greenhouse Gas Control 71 (2018) 20–35. doi:10.1016/j.ijggc.2018.02.007.

[17] J. Kita, H. Stahl, M. Hayashi, T. Green, Y. Watanabe, S. Widdicombe, Benthic megafauna and CO2 bubble dynamics observed by underwater photography during a controlled sub-seabed release of CO2, International Journal of Greenhouse Gas Control 38 (2015) 202–209. doi:10.1016/j.ijggc.2014.11.012.

[18] J. S. von Deimling, P. Linke, M. Schmidt, G. Rehder, Ongoing methane discharge at well site 22/4b (North Sea) and discovery of a spiral vortex bubble plume motion, Marine and Petroleum Geology 68 (2015) 718–730. doi:10.1016/j.marpetgeo.2015.07.026.

[19] M. Strasberg, Gas bubbles as sources of sound in liquids, J. Acoust. Soc. Am. 28 (1) (1956) 20–26. doi:10.1121/1.1908212.

[20] M. Veloso, J. Greinert, J. Mienert, M. D. Batist, A new methodology for quantifying bubble flow rates in deep water using splitbeam echosounders: Examples from the Arctic offshore NW-Svalbard, Limnology and Oceanography: Methods 13 (6) (2015) 267–287. doi:10.1002/lom3.10024.

[21] I. Leblond, C. Scalabrin, L. Berger, Acoustic monitoring of gas emissions from the seafloor. Part I: quantifying the volumetric flow of bubbles, Marine Geophysical Research 35 (3) (2014) 191–210. doi:10.1007/s11001-014-9223-y.

[22] J. Li, P. R. White, J. M. Bull, T. G. Leighton, B. Roche, A Model for Variations of Sound Speed and Attenuation from Seabed Gas Emissions, in: MTS/IEEE OCEANS 2019-Seattle, U.S., 2019, pp. 1–9.

[23] J. Li, P. R. White, R. B., J. M. Bull, D. J. W., T. G. Leighton, M. Deponte, E. Gordini, D. Cotterle, Natural seabed gas leakage -- variability imposed by tidal cycles, in: MTS/IEEE OCEANS 2019-Seattle, U.S., 2019, pp. 1–6.

[24] J. Li, P. R. White, J. M. Bull, T. G. Leighton, A noise impact assessment model for passive acoustic measurements of seabed gas fluxes, Ocean Engineering 183 (1) (2019) 294–304. doi:10.1016/j.oceaneng.2019.03.046.

[25] I. Leifer, I. MacDonald, Dynamics of the gas flux from shallow gas hydrate deposits: interaction between oily hydrate bubbles and the oceanic environment, Earth and Planetary Science Letters 210 (3) (2003) 411–424. doi:10.1016/S0012-821X(03)00173-0.

[26] J. Li, L. Liao, Y. V. Zakharov, Space-time cluster combining for UWA communications, in: OCEANS 2016-Shanghai, IEEE, 2016, pp. 1–6. doi:10.1109/OCEANSAP.2016.7485344.

[27] J. Li, DOA tracking in time-varying underwater acoustic communication channels, in: MTS/IEEE OCEANS 2017-Aberdeen, 2017, pp. 1–9. doi:10.1109/OCEANSE.2017.8084563.

[28] J. Li, Y. V. Zakharov, B. Henson, Multibranch Autocorrelation Method for Doppler Estimation in Underwater Acoustic Channels, IEEE Journal of Oceanic Engineering 43 (4) (2018) 1099 – 1113. doi:10.1109/JOE.2017.2761478.

[29] J. Li, Y. V. Zakharov, Efficient use of space-time clustering for underwater acoustic communications, IEEE Journal of Oceanic Engineering 43 (1) (2018) 173–183. doi:10.1109/JOE.2017.2688558.

[30] M. Schmidt, P. Linke, S. Sommer, D. Esser, S. Cherednichenko, Natural CO_2 seeps offshore Panarea: A test site for subsea CO2 leak detection technology, Marine Technology Society Journal 49 (1) (2015) 19–30. doi:10.4031/MTSJ.49.1.3.

[31] K. Kirk, Natural CO_2 flux literature review for the QICS project, British Geological Survey Commissioned Report, Comptes Rendus Geoscience 11.

[32] J. Lupton, C. de Ronde, M. Sprovieri, E. T. Baker, P. P. Bruno, F. Italiano, S. Walker, K. Faure, M. Leybourne, K. Britten, et al., Active hydrothermal discharge on the submarine Aeolian Arc, Journal of Geophysical Research: Solid Earth 116 (B2). doi:10.1029/2010JB007738.

[33] S. Graziani, S. E. Beaubien, S. Bigi, S. Lombardi, Spatial and temporal pCO_2 marine monitoring near Panarea Island (Italy) using multiple low-cost GasPro sensors, Environmental science & technology 48 (20) (2014) 12126–12133. doi:10.1021/es500666u.

[34] G. Caramanna, P. Fietzek, M. Maroto-Valer, Monitoring techniques of a natural analogue for sub-seabed CO_2 leakages, Energy Procedia 4 (2011) 3262–3268. doi:10.1016/j.egypro.2011.02.245.

[35] G. Caramanna, Y. Wei, M. M. Maroto-Valer, P. Nathanail, M. Steven, Laboratory experiments and field study for the detection and monitoring of potential seepage from CO_2 storage sites, Applied geochemistry 30 (2013) 105–113. doi:10.1016/j.egypro.2013.06.229.

[36] L. Beccaluva, G. Gabbianelli, F. Lucchini, P. Rossi, C. Savelli, Petrology and K/Ar ages of volcanics dredged from the Eolian seamounts: implications for geodynamic evolution of the southern Tyrrhenian basin, Earth and Planetary Science Letters 74 (2-3) (1985) 187–208. doi:10.1016/0012-821X(85)90021-4.

[37] V. M. Dekov, C. Savelli, Hydrothermal activity in the SE Tyrrhenian Sea: an overview of 30 years of research, Marine Geology 204 (1-2) (2004) 161–185. doi:10.1016/S0025-3227(03)00355-4.

[38] A. Esposito, G. Giordano, M. Anzidei, The 2002–2003 submarine gas eruption at Panarea volcano (Aeolian Islands, Italy): Volcanology of the seafloor and implications for the hazard scenario, Marine Geology 227 (1-2) (2006) 119–134. doi:10.1016/j.margeo.2005.11.007.

[39] G. Gabbianelli, P. Gillot, G. Lanzafame, C. Romagnoli, P. Rossi, Tectonic and volcanic evolution of Panarea (Aeolian islands, Italy), Marine Geology 92 (3-4) (1990) 313–326. doi:10.1016/0025-3227(90)90011-8.

[40] F. Lucchi, C. Tranne, N. Calanchi, P. Rossi, J. Keller, The stratigraphic role of marine deposits in the geological evolution of the Panarea volcano (Aeolian Islands, Italy), Journal of the Geological Society 164 (5) (2007) 983–996. doi:10.1144/0016-76492006-135.

[41] M. Anzidei, A. Esposito, G. Bortoluzzi, F. De Giosa, The high resolution bathymetric map of the exhalative area of Panarea (Aeolian Islands, Italy), Annals of Geophysics 48 (6). doi:10.4401/ag-3242.

[42] S. Aliani, G. Bortoluzzi, G. Caramanna, F. Raffa, Seawater dynamics and environmental settings after November 2002 gas eruption off Bottaro (Panarea, Aeolian Islands, Mediterranean Sea), Continental Shelf Research 30 (12) (2010) 1338–1348. doi:10.1016/j.csr.2010.04.016.

[43] A. Caracausi, M. Ditta, F. Italiano, M. Longo, P. Nuccio, A. Paonita, A. Rizzo, Changes in fluid geochemistry and physico-chemical conditions of geothermal systems caused by magmatic input: The recent abrupt outgassing off the island of Panarea (Aeolian Islands, Italy), Geochimica et Cosmochimica Acta 69 (12) (2005) 3045–3059. doi:10.1016/j.gca.2005.02.011.

[44] G. Chiodini, S. Caliro, G. Caramanna, D. Granieri, C. Minopoli, R. Moretti, L. Perotta, G. Ventura, Geochemistry of the submarine gaseous emissions of Panarea (Aeolian Islands, Southern Italy): magmatic vs. hydrothermal origin and implications for volcanic surveillance, Pure and applied Geophysics 163 (4) (2006) 759–780. doi:10.1007/s00024-006-0037-y.

[45] F. Italiano, P. Nuccio, Geochemical investigations of submarine volcanic exhalations to the east of Panarea, Aeolian Islands, Italy, Journal of Volcanology and Geothermal Research 46 (1-2) (1991) 125–141. doi:10.1016/0377-0273(91)90079-F.

[46] N. Calanchi, B. Capaccioni, M. Martini, F. Tassi, L. Valentini°, Submarine gas-emission from Panarea Island (Aeolian Archipelago): distribution of inorganic and organic compounds, Acta Vulcanologica 7 (1) (1995) 43–48.

[47] F. Italiano, R. Maugeri, A. Mastrolia, J. Heinicke, SMM, a new seafloor monitoring module for real-time data transmission: an application to shallow hydrothermal vents, Procedia Earth and Planetary Science 4 (2011) 93–98. doi:10.1016/j.proeps.2011.11.010.

[48] M. B. Porter, The bellhop manual and users guide: Preliminary draft, Heat, Light, and Sound Research, Inc., La Jolla, CA, USA, Tech. Rep.

[49] D. Jackson, M. Richardson, High-frequency seafloor acoustics, Springer Science & Business Media, 2007.

[50] T. G. Leighton, The acoustic bubble, ISBN: 0-12-44190-8doi:10.1017/S0022112094214519.

[51] G. Siedler, H. Peters, Properties of sea water, Oceanography (1986) 233–264.

[52] M. A. Ainslie, T. G. Leighton, Near resonant bubble acoustic cross-section corrections, including examples from oceanography, volcanology, and biomedical ultrasound, J. Acoust. Soc. Am. 126 (5) (2009) 2163–2175. doi:10.1121/1.3180130.

[53] E. R. Gerstein, Manatees, bioacoustics and boats: hearing tests, environmental measurements and acoustic phenomena may together explain why boats and animals collide, American Scientist 90 (2) (2002) 154–163.

[54] B. Henson, J. Li, Y. V. Zakharov, C. Liu, Waymark baseband underwater acoustic propagation model, in: IEEE Underwater Communications and Networking (UComms), 2014, pp. 1–5. doi:10.1109/UComms.2014.7017132.

[55] D. Zhou, P. Li, X. Liang, M. Liu, L. Wang, A long-term strategic plan of offshore CO2 transport and storage in northern South China Sea for a low-carbon development in Guangdong province, China, International Journal of Greenhouse Gas Control 70 (2018) 76–87. doi:10.1016/j.ijggc.2018.01.011.

[56] N. Strachan, R. Hoefnagels, A. Ramírez, M. Van den Broek, A. Fidje, K. Espegren, P. Seljom, M. Blesl, T. Kober, P. E. Grohnheit, CCS in the North Sea region: A comparison on the cost-effectiveness of storing CO2 in the Utsira formation at regional and national scales, International Journal of Greenhouse Gas Control 5 (6) (2011) 1517–1532. doi:10.1016/j.ijggc.2011.08.009.

[57] M. Claprood, E. Gloaguen, B. Giroux, E. Konstantinovskaya, M. Malo, M. J. Duchesne, Workflow using sparse vintage data for building a first geological and reservoir model for CO2 geological storage in deep saline aquifer. A case study in the St. Lawrence Platform, Canada, Greenhouse Gases: Science and Technology 2 (4) (2012) 260–278. doi:10.1002/ghg.1292.

[58] P. Teatini, N. Castelletto, G. Gambolati, 3D geomechanical modeling for CO2 geological storage in faulted formations. A case study in an offshore northern Adriatic reservoir, Italy, International Journal of Greenhouse Gas Control 22 (2014) 63–76. doi:10.1016/j.ijggc.2013.12.021.

[59] R. Chadwick, G. Williams, I. Falcon-Suarez, Forensic mapping of seismic velocity heterogeneity in a CO2 layer at the Sleipner CO2 storage operation, North Sea, using time-lapse seismics, International Journal of Greenhouse Gas Control 90 (2019) 102793. doi:10.1016/j.ijggc.2019.102793.

[60] A. Chadwick, Review confirms Goldeneye storage capability and capacity, Tech. Rep. 1, British Geological Survey (2015).
URL https://www.bgs.ac.uk/news/docs/Goldeneye_CO2_storage_Press_Release.pdf

[61] Shell, Goldeneye Gas Platform, United Kingdom. (2017).
URL http://www.offshore-technology.com/projects/goldeneye/